SANDIA REPORT

SAND2002-0701
Unlimited Release
Printed March 2002

Laser Assisted Micro Wire GMAX and Droplet Welding

P. W. Fuerschbach, D. L. Duck, L. E. Bertram, R. A. Anderson

Prepared by
Sandia National Laboratories
Albuquerque, New Mexico 87185 and Livermore, California 94550

Sandia is a multiprogram laboratory operated by Sandia Corporation, a Lockheed Martin Company, for the United States Department of Energy under Contract DE-AC04-94AL85000.

Issued by Sandia National Laboratories, operated for the United States Department of Energy by Sandia Corporation.

Available to DOE and DOE contractors from
U.S. Department of Energy
Office of Scientific and Technical Information
P.O. Box 62
Oak Ridge, TN 37831

Telephone: (865)576-8401
Facsimile: (865)576-5728
E-Mail: reports@adonis.osti.gov
Online ordering: http://www.doe.gov/bridge

Available to the public from
U.S. Department of Commerce
National Technical Information Service
5285 Port Royal Rd
Springfield, VA 22161

Telephone: (800)553-6847
Facsimile: (703)605-6900
E-Mail: orders@ntis.fedworld.gov
Online order: http://www.ntis.gov/ordering.htm

SAND2002-0701
Unlimited Release
Printed March 2002

Laser Assisted Micro Wire GMAW and Droplet Welding

Phillip W. Fuerschbach and David L. Luck
Joining and Coating Department
Sandia National Laboratories
PO Box 5800
Albuquerque, NM 87185-0889

Lee A. Bertram
Fluid and Thermal Modeling Department
Sandia National Laboratories
PO Box 969
Livermore, CA 94551-9405

Robert A. Anderson
Ceramic Materials Department
Sandia National Laboratories
PO Box 5800
Albuquerque, NM 87185-0888

Abstract

Laser beam welding is the principal welding process for the joining of Sandia weapon components because it can provide a small fusion zone with low overall heating. Improved process robustness is desired since laser energy absorption is extremely sensitive to joint variation and filler metal is seldom added. This project investigated the experimental and theoretical advantages of combining a fiber optic delivered Nd:YAG laser with a miniaturized GMAW system. Consistent gas metal arc droplet transfer employing a 0.25 mm diameter wire was only obtained at high currents in the spray transfer mode. Excessive heating of the workpiece in this mode was considered an impractical result for most Sandia micro-welding applications. Several additional droplet detachment approaches were investigated and analyzed including pulsed tungsten arc transfer(droplet welding), servo accelerated transfer, servo dip transfer, and electromechanically braked transfer. Experimental observations and rigorous analysis of these approaches indicate that decoupling droplet detachment from the arc melting process is warranted and may someday be practical.

Contents

List of Figures

List of Tables

Introduction

Laser beam welding is now widely applied throughout the world and continues to supplant traditional arc processes where high quality welding is the goal. Lasers are the heat source of choice for high reliability welding applications such as nuclear weapons, satellite devices, and medical implants. Laser welding is routine in the automobile industry for the welding of components for airbags, transmissions, and tailored blanks. Compelling reasons for the widespread success of lasers are narrow welds, compatibility with automation, and low heat input with minimal distortion.

Despite the remarkable success of laser beam welding, weld variability remains a serious problem because in implementation it is both an autogeneous and an unmanned welding process. Unlike traditional welding processes, the lack of a filler metal can lead to serious weld inconsistency since gaps along the weld joint may not be readily fused. Not only is there a lack of filler to bridge the gap, but the joint variability can cause laser energy transfer and base metal melting to decrease. Laser beam energy transfer to the workpiece is primarily due to multiple reflections (Fresnel absorption) in a molten metal cavity commonly called the keyhole. The stability of the keyhole is principal to stable energy transfer and melting. [1] In production applications where variations in joint gap and surface condition are inevitable, keyhole fluctuations have led to inconsistent welds. These problems have necessitated extraordinary measures and expense in order to maintain quality in laser welding. The strict piece part tolerances can be very costly to achieve in production and process control diagnostics must be carefully monitored to assure defects are not overlooked.

Gas Metal Arc Welding (GMAW) is a complex yet reliable welding process that is widely used in the joining of large scale components and structures in the automotive, fabrication, and metalworking industries. Metal and energy transfer from the GMAW process is not gap dependent and is set independently. The high speed and unique compatibility of GMAW with robotics has led to many productive applications in advanced manufacturing. There are two important attributes that have led to the robustness and success of GMAW. GMAW provides the ability to modify alloy chemistry locally, as required by metallurgical constraints, and also to fill the inevitable gaps along the weld joint. As presently configured in manufacturing, laser beam welding can do neither.

Regardless of the ubiquitous presence of GMAW in the fabrication industries, GMAW is seldom used for joining nuclear weapons or in other high reliability welding applications. The GMAW process has simply never been developed for welding of small scale components where fusion zone size must be strictly controlled. GMAW is regarded by many welding application engineers as a high heat input process that is incompatible with small precision devices. Although with large wire diameters heat input is necessarily high, it is not a given that heat input will remain prohibitive with very small diameter wire. Moreover, since a significantly large fraction of the arc energy is absorbed by the wire anode, [2] base metal heating can be inconsequential with small diameters.

Since both LBW and GMAW have complementary advantages as well as some singular disadvantages, it seems logical to combine the best features of both together. A hybrid process can enable extremely small, metallurgically compatible, fusion weld reinforcements to be

deposited irrespective of the weld joint gap. Since the GMAW process can provide molten metal consistently, it is straightforward to supply a corrective filler metal with the arc and assure small scale welds by precisely focusing a surface absorbed laser beam. In this way the hybrid process exhibits important features that are not obtainable with either process individually.

The important attributes of Nd:YAG laser beam welding may be especially useful with the hybrid process. In an earlier study [3] it was demonstrated that by adjusting the focused Nd:YAG laser spotsize on the workpiece one can independently increase or decrease the width of the molten weld pool. The ability to deliver the Nd:YAG laser beam with a fiber optic allows both a compact torch design and flexible positioning on the shop floor to be realized. The two main deficiencies of Nd:YAG laser welding—variable beam absorption, and defect formation, can be overcome with precise filler metal addition. In addition, the main deficiencies of micro-GMAW, namely insufficient base metal penetration and a broad high heat input, can be improved with the addition of a precisely focused laser beam..

The primary goal of this project has been to investigate and develop a laser assisted micro gas metal arc welding (GMAW) process using 250 μm diameter wire to produce miniature welds with the inherent advantages of filler metal joint augmentation and low heat input. As a first step, the development of micro GMAW welding was necessary since neither the equipment nor process understanding were readily available.

Section 1. Experiment A

Micro Wire GMAW Experimental Set-up

Micro wire gas metal arc welds were made with a 200 A micro-GMAW power supply.custom built by MacGregor Welding Systems for this purpose. A capstan driven fine wire feeder and integral torch were attached to the end of a Mitsubishi RV-E4N six axis robot to enable fully automated welding. Contact tips were acquired with a 0.33 mm internal diameter to be compatible with the 0.25 mm wire. For all welds, arc polarity was maintained with the workpiece negative and the wire electrode positive. To obtain diagnostic measurements of the metal arc transfer it was necessary to image the extremely active and luminous arc interaction zone. To observe the high intensity metal arc a nitrogen gas strobe laser was initially tried to illuminate the arc region and synchronized with a video camera that was filtered to pass only 337 nm laser light. The arc dimensions and metal transfer modes were clearly visible with this technique, but temporal detail with the integral 30 fps video camera was insufficient to observe the metal transfer event. A higher speed imaging technique was next assembled using a He-Ne laser for shadow backlight illumination and featuring a 2000 fps Ektapro EM video camera with 632 nm notch filter. This imaging system enabled clear observation of droplet detachment in the metal arc with sufficient resolution to observe transfer mode and to calculate droplet acceleration times.

Additional features of the experimental testbed included instrumentation of the welding power supply to record arc current and voltage waveforms, a high resolution encoder on the wire drive motor, and a math processing oscilloscope to record real time wire feed velocity changes.

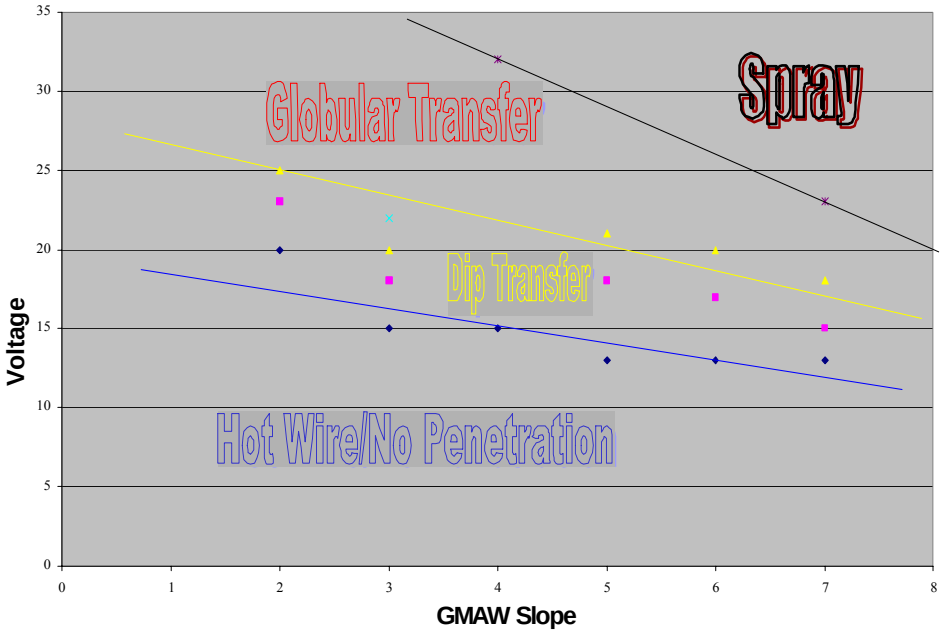

Fig. 1.1 – Chart detailing the correlation between droplet transfer mode and process variables for 0.25 mm diameter wire gmaw.

Table 1
Typical Micromig Process Conditions for Transfer

1008 steel, 1.8 mm by 26 mm by 97 mm workpiece.
Argon/2% O_2 shielding gas
0.25 mm diameter Aermet 100 filler wire,
11Ni, 13.4Co, 3.0Cr, 1.2Mo, 0.24C, bal Fe

Sample ID	CC8	CC13	CC1	S14	II	AA*	GG	24
tape counter (min.sec)	9.30	10.50	8.20	6.00	4.00	2.01	1.00	0.00
Travel Speed (mm/s)	9.0	9.0	9.0	6.0	6.0	6.0	6.0	6.0
Wire Feed speed (mm/s)	550	700	500	550	220	260	220	200
Avg. Voltage measured (V)	43.7	41.9	38.5	35.6	33.4	31.9	37.0	not meas.
Avg. Current measured (A)	78.2	63.5	49	47.5	23	18.5	21.1	not meas. 120A, 1ms
Transfer Mode observed	spray/ globular	spray	globular	dip/ globular	dip	dip	globular	globular, irregular ~ 19Hz
Avg. Power (watts)	3420	2660	1890	1690	770	590	780	not meas.
Power supply mode	80 A CC	65A CC	50 A CC	18 V CV slope 8	24A CC	22V CV slope 4	22A CC	31 A CC pulsed, 62 Hz
Linear Heat Input (J/mm)	380	300	209	280	130	100	130	not meas.
Wire Heating (J/mm)	6.2	3.8	3.8	3.1	3.5	2.3	3.5	not meas.
Cathode spot drift (mm)	8.5	6.3	6.6	6.7	5.0	4.0	5.5	5.9
Weld Bead width (mm)	4.5 some drop thru	3.7 all drop thru	3.0 no drop, ropy	4.5 some drop thru	3.0 no drop, ropy	2.2 no drop, ropy	3.5 no drop	2.0 no drop
wire stickout (mm)	0.5-1.0	1.5	2-3	n.a.	n.a.	n.a	4-9	0-2
Contact tip to work dist.(mm)	9	9	9	7.5	9	9	9	9

* some arc extinguishing occurs between shorts

For the constant voltage micro wire GMA weld tests, the type of droplet transfer mode was found to be strongly dependent on the chosen voltage and power supply voltage/current slope. The approximate relationship of observed transfer mode to set voltage and slope is given in Fig. 1.1. Typical conditions for constant current and constant voltage micro-wire welds are given in Table 1.

Micro Wire Gas Metal Arc Welds

Our first experiments with the micro-wire arc process were used to investigate the capacity and stability of droplet detachment with a small diameter metal wire. Several distinct micro-GMAW transfer modes have been photographed and analyzed using 0.25 mm diameter Ultra High Strength (UHS) steel wire. Similar modes have been observed before by previous researchers but not using the miniature wire that is unique to these experiments. [4] The extensive set of video

images as well as arc current and voltage waveforms collected in the tests documented the distinct droplet detachment modes and provided both a quantitative and qualitative understanding of the droplet detachment problem. Note the mode conditions in Fig. 1.1 and Table 1. Several judgments can be made for each mode based on our observations:

In hot wire mode the wire electrode will short to the workpiece, become softened through resistance heating, and then finally roll along the workpiece. Uniform weld bead formation is not obtained in this mode since very little heating of the base metal occurs. This mode is not practical for unassisted welding since fusion with the base metal does not occur.

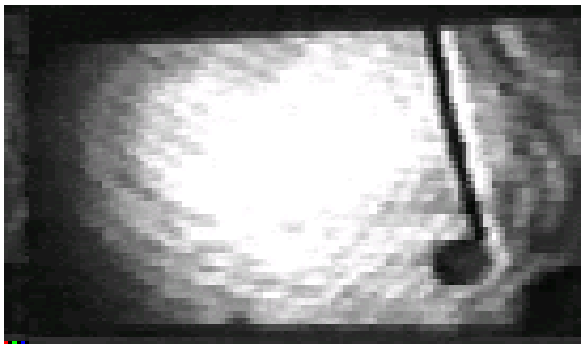

Fig. 1.2 – Video image of melt droplet forming on the end of 0.25 mm wire before dip transfer occurs. Sample II in Table 1.

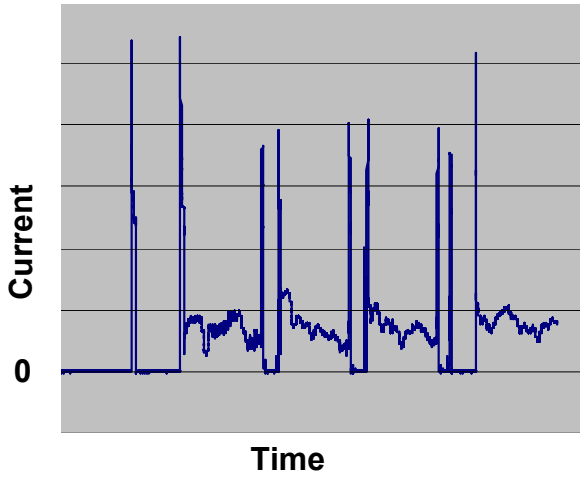

Fig. 1.3 – Oscilloscope trace of rapid rise in arc current and fall to zero when arc extinguishes in dip transfer. Sample AA in Table 1.

Dip transfer occurs when the wire is driven to electrically short to the workpiece, a rapid rise in arc current quickly melts back the wire, and the droplet is detached by strong surface tension forces. A droplet just before detachment can be seen in Fig. 1.2. Inconsistencies in droplet detachment are seen to occur because of rapid fluctuations in arc current and therefore heating. As shown in Fig. 1.3, analysis of the arc current and voltage waveforms has revealed the arc is often extinguished when the short circuit event occurs. Arc extinguishing results in an extreme fluctuation in current and melting and is a primary cause of spatter in this mode. This effect was first observed with the current waveform but was also readily verified after viewing the high speed video images.

In globular transfer the droplet forms at the tip of the electrode several millimeters above the workpiece and is periodically transferred to the workpiece by combined gravitational and electromagnetic forces at the wire tip. Not all of these droplets are uniaxially directed nor of consistent size to result in uniform bead formation. As with dip transfer, inconsistent bead formation and spatter are serious deficiencies of this mode.

In spray transfer (see Fig. 1.4), the current density on the tip of the electrode is sufficient to detach the droplet in a steady stream known as spray transfer. At high micro wire current an electromagnetic force is generated sufficient to overcome surface tension and reliably detach the molten metal droplets. Although a smooth and consistent bead is obtained in this mode, excessive heating of the base metal indicated it was impractical for low heat input applications.

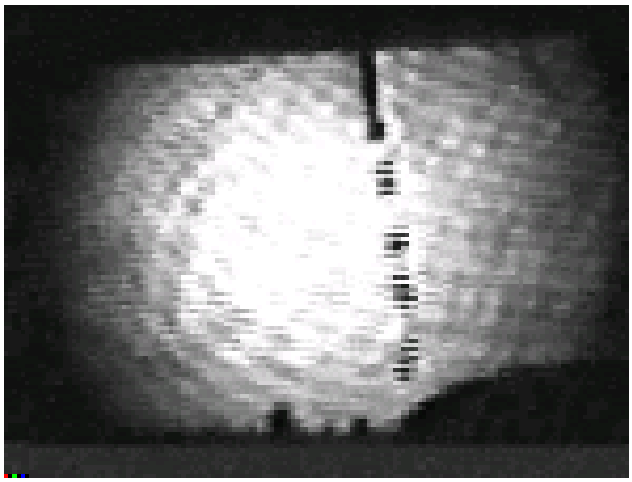

Fig. 1.4 – Video image of spray transfer mode. Molten metal droplets are seen to stream/spray from the 0.25 mm wire electrode. Sample CC13 in Table 1.

After these initial micro-wire arc process investigations, it was decided that the most promising mode of droplet detachment for laser augmentation was dip transfer since the surface tension force is strong and insensitive to arc conditions. Uniform dip transfer of the melt droplet to the weld pool can be assured if the droplet is formed and delivered to the weld pool regularly. Transferring the droplets with either spray transfer or globular transfer appears to be impractical for microwelding since the current amplitude required for these modes is too high and excessive heat input to the workpiece will result. The high currents are required in order to develop sufficient electromagnetic and vaporization forces on the droplet to achieve detachment. Common to all of the modes examined, consistent detachment of the droplet appears to be difficult and unstable enough to need improvement before an entirely successful union with laser beam welding can be achieved.

Hybrid Welds with a Micro-GMAW Arc

Hybrid laser/arc welds were completed in all of the modes described above. Base metal heating was lowest in hot wire mode as evidenced by heat affected zone extent. Promising narrow 1.8 mm wide welds were made in this mode with a smooth bead surface and full penetration into the 1.8 mm steel workpiece. Successful welds using this approach are shown in Figs. 1.5 and 1.6. Although the bead width shown in Fig. 1.6 is less than 2 mm, the weld is still relatively large when one considers that a 250 micron diameter wire electrode was used. The difficulty of transferring the filler metal to the workpiece through the arc prevented smaller weld sizes from being obtained.

Laser/Arc Interaction

Another potentially significant advantage of the hybrid process is the ability to guide the metal arc with the focused laser beam. Several references in the literature have indicated that the arc can be made to follow or even be focused by the incident laser beam. [5-7] Cathode spot drift measurements were recorded for several arc only conditions and are given in Table 1. Examination of the hot wire mode (8 V) laser/arc weld shown in Fig. 1.5 indicates that the cathode spot still wandered 3.5 mm despite the presence of the focused laser beam on the surface. From the magnitude of the drift and the high speed video images it does not appear that any substantive interaction between the laser beam and the arc occurs; which is to say that no dramatic change in position, heat affected zone, or weld profile has been detected beyond what one would expect due to the additional presence of a high power heat source.

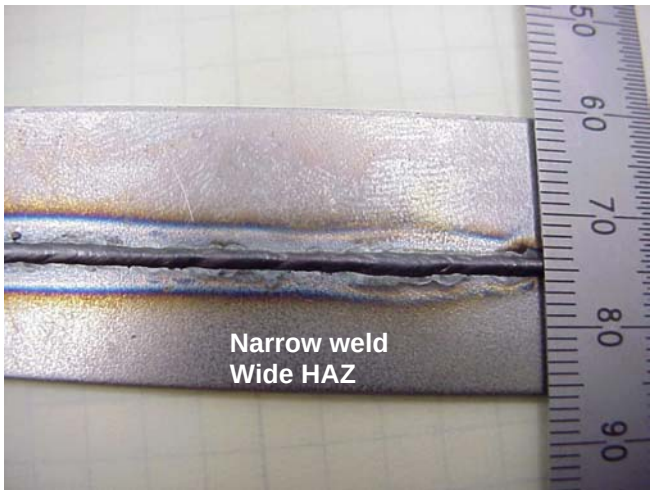

Fig. 1.5 - Laser assisted micro GMA bead on plate weld, 1008 steel sheet. Hot wire transfer mode. Ar-2%O_2 shield.

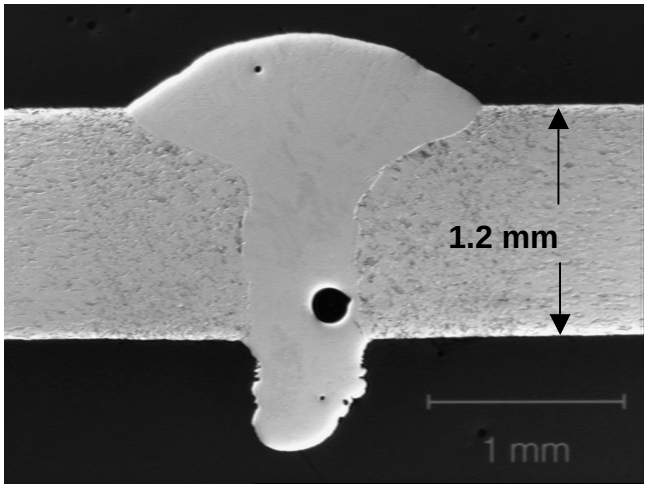

Fig. 1.6 – Metallographic cross-section of weld in Fig. 1. 1000 W Laser, 8 V constant voltage arc, 18 mm/s travel speed, 250 mm/s wire feed speed

In an earlier report for laser/plasma arc welding, nailhead like welds were made that were similar to the weld cross-section shown in Fig. 1.6.[8] It was concluded that if the fusion zone width was not enlarged below the surface, then the arc was not focused or directed down into the keyhole by the laser beam, and an important laser/arc synergy did not occur. Although focusing of the arc by the laser was also not observed in this study, nonetheless it cannot be ruled out for conditions other than those examined here. There may indeed be process conditions and applications where the presence of the laser beam does influence the arc characteristics.

A remarkable laser/droplet interaction was observed in globular transfer as propelled metal droplets were impacted by the focused laser beam and were either repelled 180°, or their path was significantly altered. This phenomena is thought to be due to significant vaporization from the face of the molten droplet when impacted by the focussed laser beam. This is believed to be the same vaporization force that maintains a stable vapor cavity or keyhole in deep penetration laser and electron beam welding.

Section 2. Micro Wire GMAW Theory Development

Some Scaling Issues for GMAW Welding

We start with the "base case" of GMAW using 30-62.5 mil (0.001 in) steel wire, at welding conditions which work well at producing a smooth, constant width bead (Fig. 2.1). Then, in order to obtain some guidance on how to develop parameters which can produce an equally successful weld when using 10 mil wire, we examine the way in which these parameters change when size is reduced.

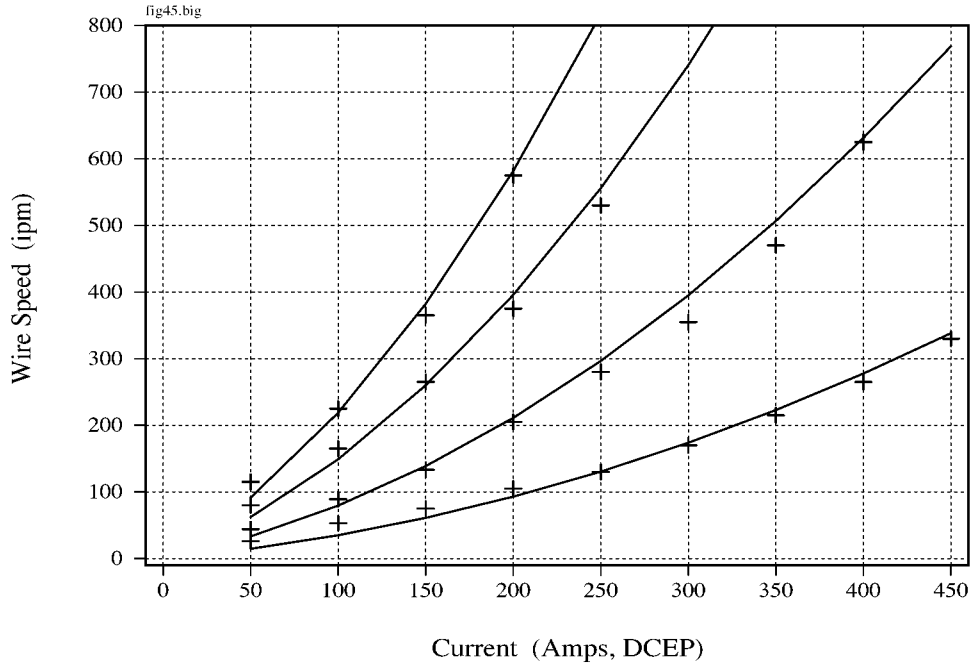

Fig. 2.1. Experimental weld parameters from *Welding Handbook*[9] [Fig. 4.5]. Constant Voltage, Electrode Positive weld parameters (current and wire feed speed) on mild steel for four different size wires are shown as + symbols. These are fit by Eqs.(1) and (2) of the text, which plots as the solid curves.

Presuming that the heating of the wire occurs due to a fixed anode fraction of the arc power, plus an Ohmic heating portion, one can write for the wire speed V_w:

$$V_w = aI_a + bLI_a^2 \qquad (1)$$

where arc current is I_a and wire stickout beyond the contact tube is L; a and b are constants for a given wire alloy, wire diameter d_w, travel speed V_o, and power supply setting (open circuit voltage and slope). By assuming that the stickout was constant at L_o for the cases plotted in Fig. 2.1, and that the coefficients a and b have a power-law dependence on d_w, we obtain the fit shown in Fig. 2.1 for :

$$a = 10^{-3.64}\ d_w^{-2.5}\ \text{(ipm/A)} \quad \text{and} \quad b\ L_o = 10^{-5.95}\ d_w^{-2.5}\ \text{(ipm/A}^2\text{)} \qquad (2)$$

This fit can then be used to predict the settings needed for thin wire, as shown in Fig. 2.2.

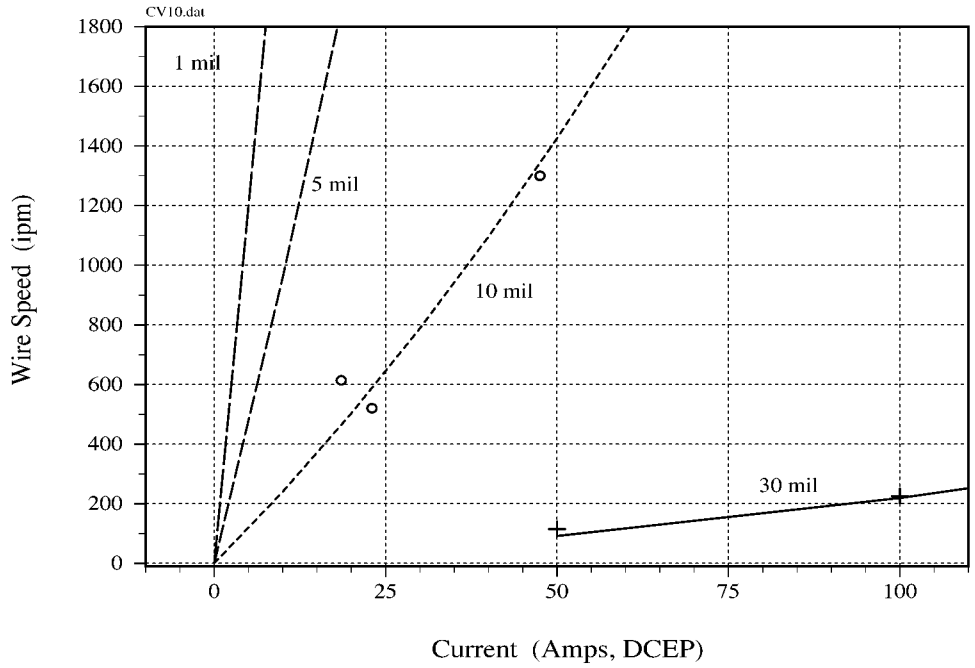

Fig. 2.2. Extrapolation of curve fits in Fig. 2.1 to thin wires, 1-10 mil diameters. Open circles near the 10 mil wire curve show experiments. Since that extrapolation succeeds, use Eqs. (1) and (2) to estimate conditions needed for 5 mil wire and 1 mil wire. Clearly, 5 mil case is difficult, and 1 mil case would require custom power supply and wire feed, if its 'single ecton' arc could be maintained.

To the degree that the extrapolation in Fig. 2.2 is valid, it calls for very small currents to operate at 5 mil or 1 mil wire size. In fact, detailed studies of arc physics have shown that currents of a few A operate with a single cathode spot, which jumps from one cratering event to the next as it travels. These cratering events have been labelled 'ectons' [10], and are the subject of active research today[11].

Ecton motions on clean metal surfaces in vacuum consist of a general trend, about which a great deal of random meandering takes place. This meandering increases the risk of arc extinguishment, and spreads the heating of the cathode surface over an area much larger than the spot size (which is typically less than 100 μm). For both reasons, a good weld will require the meandering be brought under control.

Since the ectons leave a visibly modified surface behind, it is not difficult to assess the scale of the meandering for the experiments with 10 mil wire. This has been done by eyeball and recorded in Table 1 as 'cathode spot drift'. That data makes it apparent that the scale of the meandering in the Ar gas atmosphere of the weld is comparable to the contact tip-to-workpiece

distance rather than the wire diameter; i.e., 15-20 d_w was the typical meander width. For true 'microGMAW' performance, we desire that this be reduced by an order of magnitude.

Ideal MicroGMAW?

Before exploring further issues of scaling of the GMAW process, we should state some specific criteria which define a desirable micro-GMAW weld. A strawman scenario is sketched here. The scale reference which arises naturally, as in the above discussions, is the wire size d_w. As this is reduced, geometric similarity would require that the workpiece thickness t_{wk} and weld bead width w would reduce in proportion. For metallurgical equivalence, the width of the heat affected zone w_{haz} might be also desired to reduce in proportion. These criteria may very well prove to be overconstraints on the process variables, since, as seen in the analysis above, the arc physics has its own imperatives for partitioning the energy deposition between wire and workpiece.

Another weld parameter which might be expected to scale geometrically is the contact tip-to-workpiece distance. The experiments in Table 1 indicate that a comfortable reduction by a factor of 2 between the typical 20 mm distance for 0.035 in dia wire, to 9 mm for the 0.010 in dia wire, was used. For strict geometric similarity, a distance of 5mm or so would be needed.

A typical GMAW application today, as displayed in Table 4.8 of the Welding Handbook, has a workpiece thickness of 1.8-7 wire diameters, and is presumably producing a bead of about this width (2-10 diameters, say). Accordingly, we should be seeking a similar range of bead widths in the micro-GMAW welds. The workpiece in the experiments was about 7 wire diameters thick, but weld bead width was a bit above the geometric similarity value (12-15 diameters).

Metal Transfer Modes and Scales

The qualitative background observations noted along the way in this discussion are from high speed video of GMAW made at Sandia Livermore by Beth Fuchs and Alan Pomplun, and the high speed video images of the 10-mil GMAW experiments given in Table 1 above.

The first observation is that experience indicates that the metal transfer is not a smooth process, but rather proceeds by forming droplets of molten metal on the wire end, which subsequently detach and are deposited on the workpiece. The modes by which this can occur, in order of increasing current and wire speed, are 'short-circuiting' (called "dip" for short in the table; pun noted), 'globular', 'spray', and 'streaming' transfer.[9,12,13] We start with a discussion of 'globular' transfer in which a single droplet, larger in diameter than the wire, melts before transfer occurs, because this is the most frequent entry in the micro-GMAW table above.

In Fig. 2.3, the typical parameters for a GMAW weld on mild steel using 35 mil wire are shown, for the globular transfer case. The lengths are scaled to the wire diameter in this plot, so that we can examine geometric similarity of the micro-GMAW welds to this 'nominal' case, as shown in Fig. 2.4. Clearly, the scaling of the welds is not strictly geometric for the currents and wire speeds so far examined experimentally.

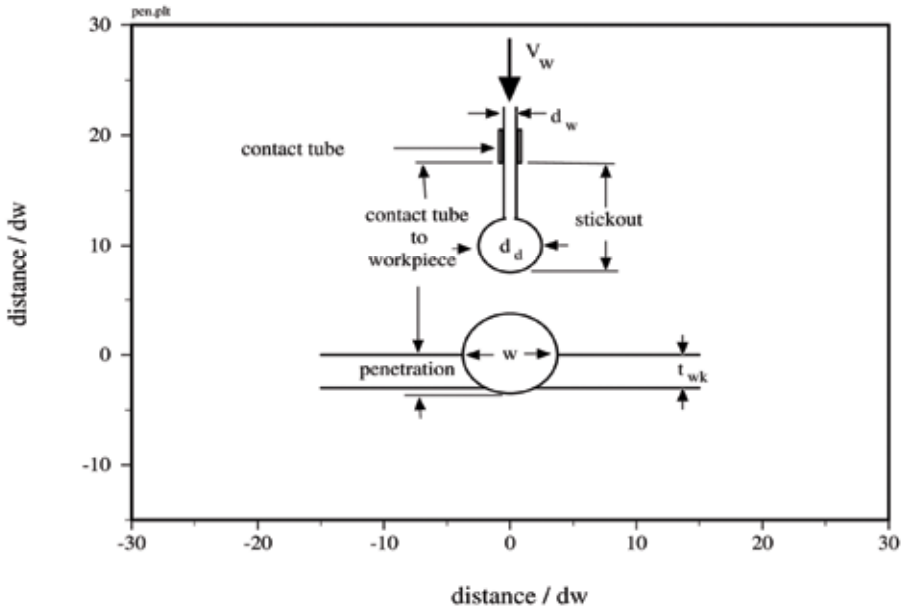

Fig. 2.3 Nomenclature for GMAW bead-on-plate weld, with drawing to scale for 0.035 in dia wire on mild steel.

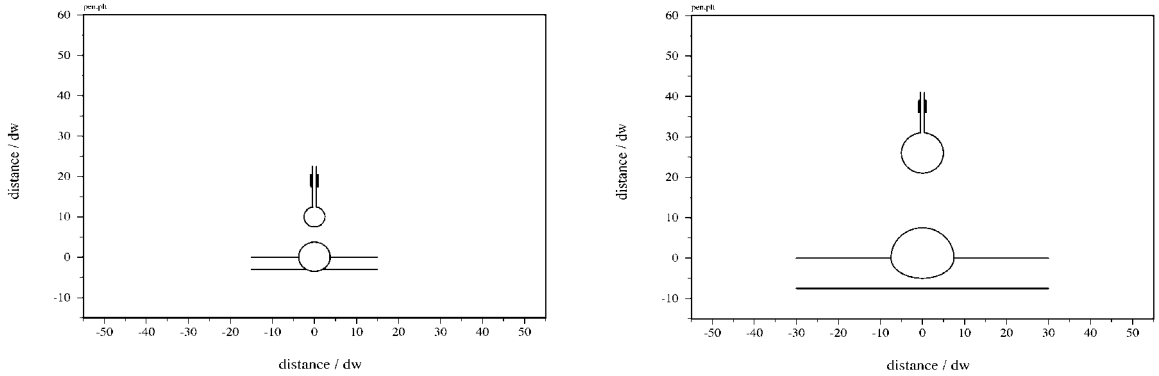

Fig. 2.4 (a) Same as Fig. 2.3, in larger frame. (b) Typical micro-GMAW weld, in same frame as Fig. 4(a). Length unit is one wire diameter in both (a) and (b), with micro-GMAW being 10 mil wire. Note larger globule, thicker workpiece and partial penetration weld in (b), all of which are signals of lack of geometric similarity.

Despite the lack of geometric similarity in the welds reported above, we can note that conserving metal volume as the wire melts into the bead results in the simple relation:

$$V_o = V_w \left(2d_w / w \right)^2 \qquad (3)$$

when the bead is of width w and is semicircular. This means that once a wire feed speed and current are chosen by Eqs(1,2), choosing bead width w results in a forward travel speed V_o given by (3). The data of the table verify this relation with a couple of exceptions. Thus, (3) can be used to guide future experimental parameter choices if it is desired to improve the geometric similarity between nominal GMAW and micro-GMAW welds.

A second basic scaling question is the issue of energy partition: as wire size changes, how does the fraction of energy deposited on the wire to melt it change? Since (1) and (2) provide the basic scaling rule, we can write:

$$\rho_m \frac{\pi}{4} d_w^2 V_w \Delta h_m = \eta_w I_a V_a$$

to define η_w, the fraction of input power going to melt the wire. This has been measured by calorimeter in the nominal case [11] and found to be around 0.40. From that value and Eqs(1,2), it follows that the superheat in the droplets must be around 350-375K for the 35 mil wire, so that the enthalpy change from room temperature to the droplet temperature is Δh_m = 1475 J/gm. If the superheat is the same for 10 mil wire, then its value of η_w = 0.34 is somewhat smaller, even though the scaling (2) indicates that it will go as $1/\sqrt{d_w}$. Offsetting this factor are the terms in the ratio $(1 + I_a / 206A)/V_a$, with the net effect of reducing η_w for the smaller wire.

The relatively larger globule in Fig. 2.4(b) raises the question "what criterion determines how large the drop will be when it detaches in globular mode?"

Supposing that the droplet is attached to the wire by its surface tension force, and is acted on by volumetric forces (weight and electromagnetic) and surface forces (aerodynamic drag and arc reaction forces), we can write a balance of these forces at the moment of detachment as:

$$\pi d_w \sigma = \frac{1}{6} \pi d_d^3 \rho_m \hat{g} + \frac{1}{8} \rho_s V_s^3 C_f \pi d_d^2 + \frac{1}{4} S_{EM} \pi d_d^2$$

where $\hat{g}$ is the acceleration due to gravity plus an appropriate electromagnetic term, and S_{EM} is the electromagnetic reaction force per unit area averaged over the droplet section. These coefficients depend on the geometry, but are assumed to have weaker dependence than the areas and volumes, which are quadratic and cubic in the size d_w of the wire. Solving this relation for the droplet size d_d results in an approximate relation:

$$\frac{d_d}{d_w} = \left[\frac{n_{dst}}{1 + n_{da} n_{dst}^{-1/3}} \right]^{1/3}$$

in terms of the dimensionless numbers:

$$n_{dst} = \frac{6\sigma}{\hat{g} d_w^2 \rho_m} \quad \text{and} \quad n_{da} = \frac{3}{4} \frac{\rho_s V_s^2 C_f + 2 S_{EM}}{\rho_m \hat{g} d_w}$$

which characterize the ratios of surface tension force and surface forces, respectively, to the volumetric forces on the droplet. In the case with $n_{da} << n_{dst}$, that is, surface tension dominant, then d_d varies as $d_w^{1/3}$, a weak dependence. In particular, changing wire size from 45 mils to 10

mils would reduce the globular droplet radius by 39% if this scaling rule were exact; this represents a mass change proportional to the wire diameter change—4.5 times smaller. This ratio can be observed in the high speed images of both the 35 mil case and the 10 mil case. From high-speed movies, we know that excessive travel speed V_o in GMAW results in depositing a chain of distinct droplets rather than laying down a continuous bead.

Section 3. Experiment B - Other Droplet Detachment Methods

Background

After significant effort to develop consistent droplet detachment techniques a fundamental limitation of gas metal arc welding with small diameter wire became apparent. The droplet detachment and propulsion process requires a much higher level of arc thermal power than is desired for most miniature welding applications. Stable transfer was only obtained at arc power levels that result in extensive and impractical workpiece heating. Despite the efforts detailed above, metal arc welding has not been scaled down to the dimensions required to be considered a low heat input welding process. Consequently, decoupling wire melting from base metal heating became a primary design goal for the project. Several approaches to decouple droplet detachment from workpiece heating were considered. Four promising droplet detachment methods that were investigated experimentally will now be described:

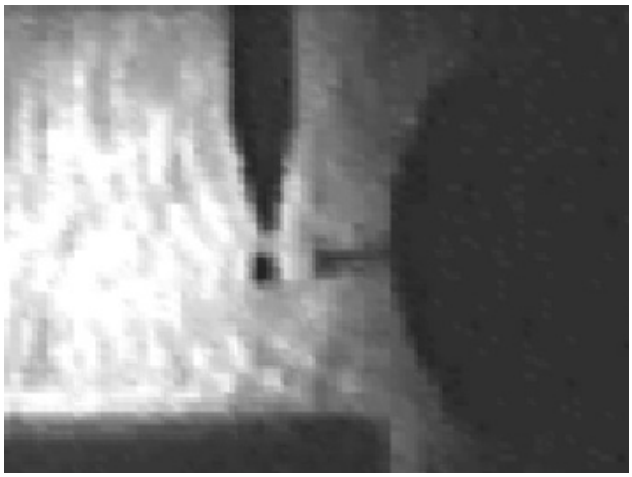

Fig. 3.1 - High speed video still image of pulsed tungsten arc transfer. Droplet has just melted off the horizontal wire and is moving down towards the workpiece.

Pulsed Tungsten Arc Transfer (Droplet Welding)

Droplet Welding in the manner examined here (Pulsed Tungsten Arc Transfer) was originally demonstrated by Suslov to be effective in detaching and directing small spherical molten droplets. [14] Pulsed Tungsten Arc Transfer was investigated since it possesses the important advantages of low heat input and small droplet size. The method relies on pulse current arc forces in a detached tungsten arc to propel a molten metal droplet to the workpiece. Droplet formation occurs in an isolated tungsten/wire arc above the workpiece as shown in Fig. 3.1. The pointed electrode negative tungsten concentrates the arc energy exclusively on the forming droplet. Unlike gas metal arc welding where extensive heating of the workpiece is required to obtain droplet melting and detachment, this approach enables a complete decoupling between the arc electrode melting and the workpiece heating. The arc is simply required to produce enough energy to melt the droplet. With the addition of a focused laser beam, cleaning, surface melting, melt-in, and penetration of the workpiece, can all be attained independently of the arc. Detached droplet formation should enable small heat affected zones and miniaturization of the process.

As for the earlier micro wire GMAW experiments, a laser backlighting testbed was assembled with a high speed video camera to record droplet motion. A Macgregor Welding Systems model PA100 pulse arc power supply was used to precisely melt the tip of a 0.25 mm wire, form a molten droplet, and simultaneously detach it. A 1.0 mm diameter lanthanated tungsten with a 30° tip angle was employed vertically as the negative electrode. The horizontal electrode positive wire was indexed manually after each pulse and connected to the power supply with the same

copper contact tip used for the micro GMAW experiments described earlier. Typical pulse parameters were 70 A current for 2 ms with Argon shielding.

Testing with this set-up revealed that the droplet could not be consistently propelled to the chosen workpiece location. Variations in initial tip condition were found to significantly affect the detachment. Depending on the size of the detaching droplet the subsequent tip condition could be either be sharp edged or partially melted. The degree of melting during the next pulse was then variable as was the detachment event. This approach also required that the small diameter wire be located precisely near the 1.0 mm tungsten tip. The volume of wire melting was significantly affected if the initial wire position was not exact. A separate control servo to maintain exact wire position was needed and dismissed due to time constraints and the development complexity. Precise droplet positioning with this method is clearly problematic and other more promising detachment methods were instead investigated.

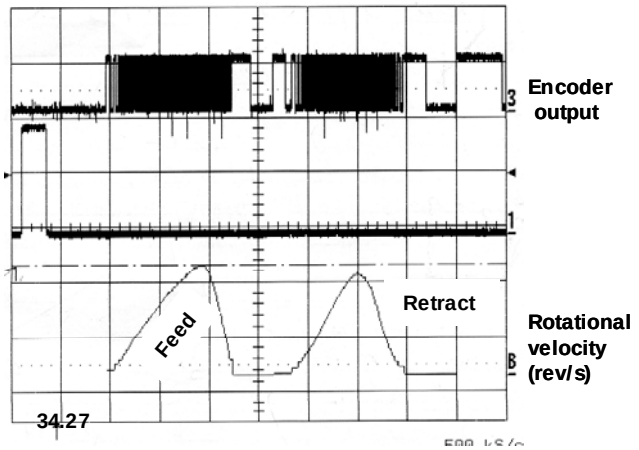

Fig. 3.2 – Oscilloscope trace of encoder pulses and wire velocity versus time. The programmed rapid change in velocity was used to detach droplet in Servo Accelerated Transfer.

Servo Accelerated Transfer

Mechanical control of the feed wire potentially can detach the droplet independent of the arc power as soon as a droplet is formed on the electrode. This approach is advantageous because a high arc current is not required and also because detachment can be independent of gravity. Mechanical vibration with cams, electromagnets, gas flow pulsation, and other methods have all been successfully demonstrated by others.[15-18] Those methods employed much larger diameter wire electrodes and have not been commercially developed in the U.S. With the advent of programmed servo motor controls it is now possible to obtain fast acceleration of the wire with almost any motion characteristic desired. Since feed wire motion must be controlled in any case, it seemed logical to try to drive the wire in a manner to release the droplets when required.

We investigated using a servo motor to rapidly accelerate a droplet formed on the end of the torch feed wire and thereby obtain detachment by mechanical force on the wire/droplet. Rapid motion of the wire was obtained with a computer controlled brushless servo motor (Compumotor model BE33) that accelerated and de-accelerated the wire after each current pulse in the detached arc. A typical wire velocity droplet detachment cycle can be seen in Fig 3.2. The wire direction, acceleration, and amplitude were set via PC control software that was used to drive the motor. Recording of the encoder output enabled the quantitative display of actual wire motion shown in Fig. 3.2.

As was the case for pulsed tungsten arc transfer described earlier, it was observed from the high speed video images that the initial condition of the wire tip was critical in determining the direction of the droplet motion. If the solid tip was not square across the end, the droplet was

propelled at some angle away from the direction of wire travel. Since arc wandering can affect the degree of melting across the tip, uniform tip melting may always be difficult to obtain with this approach.

The most important and demanding problem with this method was that stable and consistent detachment could only be obtained with large drop diameters. Only when the droplet reached a critical mass was the acceleration force sufficient to overcome the surface tension force and detach the droplet from the wire. Modifications to the servo motor drive system and software were not sufficient to obtain wire accelerations greater than 10 *g*. From our analyses of high-frame-rate video recordings, it appears that small droplets can remain attached at much higher effective accelerations. We found examples of oscillatory droplet motion along the wire axis at approximately 200 Hz, with oscillation amplitudes that implied peak accelerations of at least 50 *g*.

The acceleration obtained with this servo motor appears to be the maximum feasible for that servo type. It is therefore thought that up to 100 *g* accelerations would be necessary to obtain consistent droplet detachment. To scale the process down for very small diameter wires is even more difficult because the surface tension force that would need to be overcome decreases only linearly as the wire diameter decreases. By contrast, the inertial forces on a droplet vary as the droplet mass, which is proportional to the cube of the droplet diameter. Therefore, for a fixed wire acceleration, the ratio of surface tension and inertial forces rapidly increases as the wire and droplet diameters both decrease.

Servo Dip Transfer

Pulsed tungsten arc transfer showed that a detached arc can provide consistent droplet formation under many conditions. A potentially more consistent variant of pulsed tungsten arc transfer was envisioned using surface tension to detach the droplet by precisely indexing the wire after droplet formation. After droplet formation, the wire electrode is rapidly positioned until contact with the workpiece is made. Upon sensing workpiece contact the wire feed system retracts the wire electrode and repositions the tip near the tungsten for the next arc pulse.

We were confident of this approach having earlier observed surface tension transfer to be an extremely effective detachment method with micro wire GMA in the dip transfer mode. Servo Dip Transfer seemed well suited to laser/arc processing since the focused laser can readily provide all of the workpiece heating necessary to achieve smooth melt-in of the filler metal. By closed loop control of the wire feed displacement the process can be self regulating which is a fundamental advantage of conventional GMAW. This approach was also expected to be quite scalable and could be used with both very fine and very large diameter wires.

The method investigated (shown in Fig. 3.3) relied on a detached tungsten (electrode negative) arc for droplet melting but used a servo motor to drive the wire and attached droplet to the required location on the workpiece where the laser beam was focused and a weld pool already formed. Droplet formation was obtained on the (electrode positive) wire end by maintaining a 4 A low current arc and periodically pulsing the current (120A, 1 ms, 5 pps) at a low duty cycle to form the droplet on the tip. The weld wire was fed and retracted after each current pulse in a manner similar to that of manual GTA welding. To prevent the wire from melting beyond the tip, a 0.5 mm diameter wire was required along with a background current below 5 amperes.

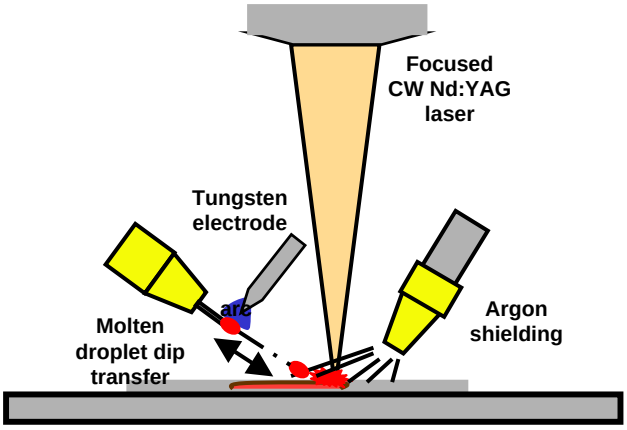

Fig. 3.3 – Schematic representation of wire melting, laser heating, and droplet placement in Servo Dip Transfer.

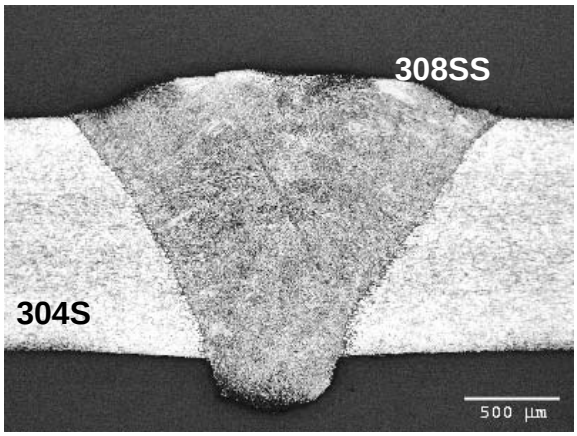

Fig. 3.4 – Metallographic cross-section of hybrid 304 stainless steel weld made using Servo Dip Transfer. 7.6 mm/s, 1500W Nd:YAG, 5 pps, 7.6 mm/s

Although this approach was quite technically challenging, encouraging welds were obtained. As expected the droplet was readily detached to the laser formed weld pool each time the wire tip was indexed. The process was also observed to be self regulating. When the molten droplet was not indexed far enough to meet the weld pool, a much larger droplet formed after the next pulse was easily detached since it was of a larger diameter and easily touched the molten pool.

It was found that a significantly large weld pool was required in order to obtain consistent droplet detachment. To obtain a large weld pool with the continuous wave Nd:YAG laser (1500 W) a slow travel speed (7.6 mm/s) was necessary. As a result, the welds obtained were not significantly smaller in size than welds obtained with more conventional laser and arc processes. The servo dip transfer weld shown in Fig. 3.4 does however indicate that the hybrid process is able to penetrate deeper than is typical for a conventional arc welding process.

Since Philips[19] has been successful in obtaining copper droplet wetting on solid surfaces with molten droplets, it was anticipated that droplet attachment with servo dip transfer might not require a molten weld pool to be successful. The Philips detached arc process does not affect the workpiece surface but instead assures wetting by superheating a droplet on the end of the feed wire with a high current pulse. The addition of a laser beam in this experiment to clean and preheat the workpiece was anticipated to further improve surface wetting.

It was observed that no satisfactory detachment could be achieved without a molten pool present. The droplets would not detach from the wire and were flattened on the side that impacted the workpiece. The laser beam did not suitably prepare the sample surface to enable direct detachment of 308 SS metal droplets to either a 1008 steel or a 304 SS workpiece. Preheating of the substrate and exposure to the focused laser beam was not sufficient to break down the surface oxides and enable droplet attachment. It was observed that the focused laser beam diameter on the workpiece was relatively small relative to the droplet size. Defocusing the laser beam thereby increasing the beam diameter did not improve the situation since it reduced the beam intensity such that little surface vaporization and cleaning could be obtained.

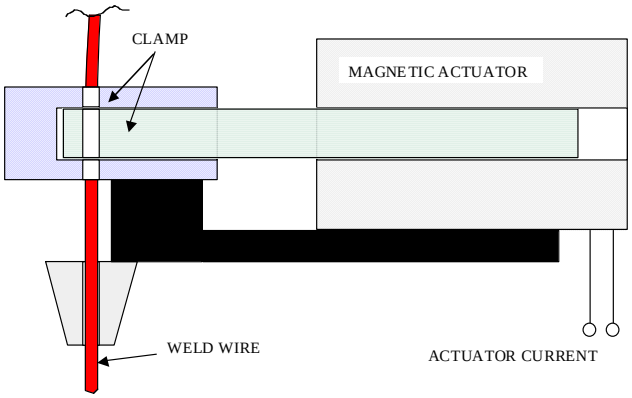

Fig. 3.5 – Schematic of electromechanical wire brake mechanism used in Method D.

Electromechanically Braked Transfer

When one considers inertial droplet detachment, it is clear that the wire motion should result in droplets that are moving toward the workpiece when they are released. Accordingly, a cycle of wire extension and retraction may not be desirable. An alternative would be to accelerate the wire toward the workpiece and then instantaneously halt that motion when the droplet is co-moving with the wire, with the intent that the droplet would continue to move and break free from the wire end.

A simplified view of the surface tension force helps to understand this detachment scheme. We imagine that the restoring force can be approximated as an ideal spring with viscous friction, so that the droplet motion relative to the wire is an under-damped sine wave that is excited by wire accelerations. If the wire motion is suddenly arrested, the peak inertial force subsequently experienced by the droplet is proportional to the droplet velocity at the instant the droplet moves beyond the end of the wire. If we adopt a resonant frequency of 200 Hz, it is readily calculated that an initial droplet velocity of approximately 800 mm/s would be needed to achieve an acceleration of 100 *g*. Because this velocity is near that already available from the serve motor drive system, we were encouraged that consistent droplet detachment might be achieved by synchronizing a fast-acting electromechanical brake with the drive system cycle and tuning the cycle frequency to the droplet motion resonance. Achieving optimal conditions, of course, would require substantial experimentation.

Figure 3.5 depicts our electromechanical brake concept. The wire passes through slightly larger diameter holes in a lightweight movable piston between stationary frame members. A very small retraction of the piston clamps the wire by gentle shearing forces. In our prototype the actuator was a small relay electromagnet and the moving part was attached to the relay paddle through an electrically insulating coupling.

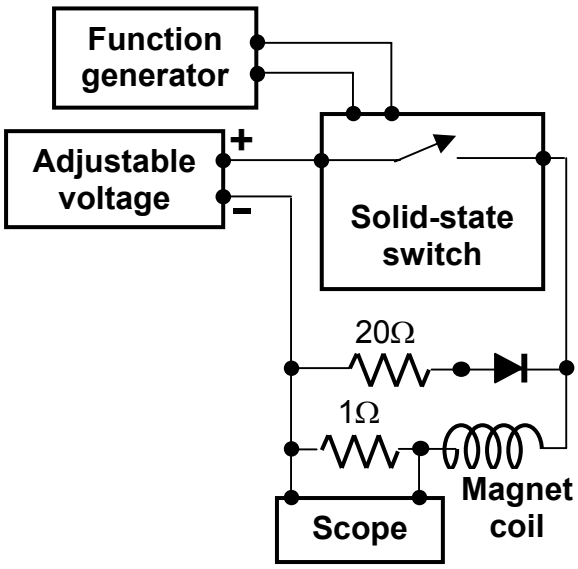

Fig. 3.6 - Passive control circuitry used to energize the electromechanical wire brake.

The passive control circuitry used to test the wire brake prototype is shown in Fig. 3.6. The function generator produced an asymmetrical square wave at 20 Hz which gated the solid-state switch. Our magnet coil had a resistance of 14 Ω and an inductance of about 0.1 Hy, giving a current risetime of the order of 10 ms, and a current of about 1 A produced ample clamping force. The diode prevented overvoltage damage when the solid-state switch was

gated off, and the 20 Ω series resistance hastened the decay of current. By adjusting the function generator duty cycle and the power-supply voltage, we were able to achieve a narrow, roughly triangular, current pulse.

In the initial experiments the wire drive was set a constant speed, and high-frame-rate video recordings verified that the wire motion was briefly interrupted at 50 ms intervals. Our first attempts, however, did not demonstrate reliable droplet detachment. A faster response from the electromechanical brake would have been desirable, because that would have allowed higher cycle frequencies. An active control circuit might have enabled this.

An alternative use of this wire-braking concept would be to arrest the wire motion, in dip-transfer welding, the instant the droplet electrically contacted the workpiece. This would prevent the weld wire from penetrating too deeply.

Section 4. Droplet Attachment Theory Development

Droplet Heating of a Workpiece

Suppose we have a source of droplets of molten alloy producing droplets of diameter d_d at intervals of t_d, and these are ejected from the point of creation with velocity V_d and superheat $T_{\sup}$. These parameters characterize the droplet stream, and are presumed known as a function of the process settings. For instance, if the source is the Philips process[19] or the micro-GMAW process described in section 2, these values are determined when a given wire feed speed V_w and arc setting (current, voltage, pulse rate, intensity, and mechanical acceleration) are specified. For Laser Engineered Net Shaping (LENS)[20] or plasma spraying, different settings fix these values.

This stream of droplets is to be deposited on a workpiece, which will be presumed to be a flat sheet of some alloy, perhaps different than the droplet alloy. In that case, the superheat is the difference $T_{\sup} = T - T_m$ where T_m is the meltpoint of the workpiece alloy. For LENS, $T_{\sup}$ is usually negative—the particles are still solid when they enter the melt pool on the workpiece.

The goal in micro-GMAW is to deposit these droplets on the workpiece to produce a bonded joint, with some penetration p of fused metal. From the desired p and the four parameters for the droplets $d_d, t_d, V_d, T_{\sup}$ the following analysis will provide the amount of auxiliary thermal power P_a which must be provided to allow production of a 'bead on plate' joint at some travel speed V_o.

At the outset, two quite different regimes are defined for the case when penetration p is much larger than d_d (small droplets being engulfed in a large pool), or not. This small droplet regime is 'LENS-like', and, in the case of molten droplets, might be called 'Liquid LENS' or 'LLENS'. Here, the full thermal power of the droplets, and their mass, is captured by the pool. This will be considered as a special case of microGMAW aftter the analysis which follows.

When penetration p is comparable to the droplet size d_d, we have the microGMAW scenario depicted in Fig. 4.1. Molten droplets land on the (barely) solid workpiece, and conduct heat to it with power

$$P_d = m_d \, C_{pd} \, T_{\sup} / t_d \qquad [1]$$

where the droplet mass is $m_d = \frac{4}{3}\pi\left(\frac{d_d}{2}\right)^3 \rho_d$ and its specific heat is C_{pd}. This is a reasonable approximation so long as the time t_d is adequate to allow heat conduction into the workpiece. It will be usual for the droplet to have a vigorous internal circulation due to surface tension and the violence of its production, so its internal temperature will be assumed uniform in this discussion.

To build up a continuous bead of the droplets, they must undergo a deposition process which converts them into overlapping globs as depicted in Fig. 4.1. For hemispherical globs, with overlap along the centerline of deposition of f_{ol}, the travel speed V_o of the workpiece relative to the source must be:

$$V_o = (1- f_{ol})\, d_d \,/ t_d \qquad [2]$$

Thus, the kinematic requirement that the bead be continuous provides estimate [2] for V_o in terms of the droplet source parameters.

Power P_{tot} deposited at a stationary point on a halfspace produces a steady state pool (after infinite time) bounded by the melt isotherm T_m, with radius r_∞, where

$$P_{tot} = 2\pi\, r_\infty\, k\, T_m \qquad [3]$$

where k is the thermal conductivity of the workpiece. When droplets are small, the conductive solution for temperature in the workpiece should be a good approximation, so Rosenthal and Rykalin solutions are used henceforth to relate the penetration to the lengthscale r_∞.

The most convenient way to write the Rosenthal/Rykalin solution for a moving point source is dimensionless form. Thus, a penetration parameter $G_r = A_{pen}/(\frac{1}{2}\pi\, r_\infty{}^2) = p^2 / r_\infty{}^2$ given as a function of the dimensionless travel speed ('Rykalin number') $R_y = V_o\, r_\infty / 2\,\kappa$ is one form for the solution for heat conduction in the workpiece[21-23]

$$G_r = A_{pen}/(\frac{1}{2}\pi\, r_\infty{}^2) = \text{fcn}\ (R_y) \qquad [4a]$$

where κ is the thermal diffusivity of the workpiece $\kappa = k / \rho\ C_p$. Because the design problem implicit in Eqs. [1-3] considers the droplet parameters and penetration as independent variables (to be chosen freely), the power input becomes a dependent variable, and it is more convenient to recast Eq.[4] in the form:

$$\frac{r_\infty}{p} = F\left(R_p\right) \qquad [4b]$$

where $R_p = R_y \frac{r_\infty}{p}$ is a Rykalin number based on penetration, appearing as the independent variable. The solution $F\left(R_p\right)$ is closely approximated by:

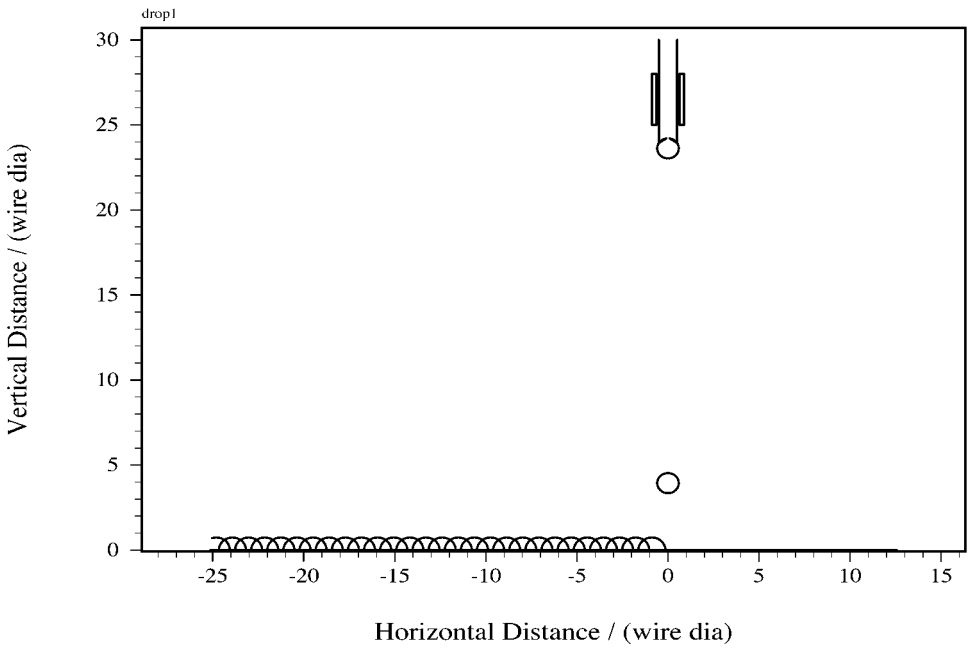

Fig. 4.1. Example case of micro-GMAW welding using 10-mil wire. The contact tube is stationary, while the workpiece moves to the left at the travel speed. Droplets of 11.8 mil diameter are produced at 0.02 sec intervals (50 Hz) and ejected with 9.84 inch/sec (25 cm/sec) velocity toward the workpiece at superheat 2520 deg F (1400 K). Droplets impact with 25% overlap, requiring workpiece travel speed 26.57 ipm (1.125 cm/sec) according to Eq.[2]. The droplets conduct power 4.6 W to the workpiece according to Eq. [1], and penetration of 5 mils combines with the travel speed to make R_p = 0.1107. In [4b], the point source heat conduction solution would have r_∞ = 1.068 p ; that value requires auxiliary power 31.2 W in Eq.[5b].

$$F(R_p) = \begin{cases} 1 & \text{for } R_p < 0.0316 = 10^{-3/2} \\ 0.515229\ R_p^f & \text{for } 10^{-3/2} < R_p < 10 \\ R_p & \text{for } R_p > 10 \end{cases} \qquad [4c]$$

where $f(R_p) = \frac{24}{125} + \frac{16}{125}\left(\log R_p + 3/2\right) + \frac{4}{125}\left(\log R_p + 3/2\right)^2$ gives exponent f .

Approximation [4c] takes a simple form for very slow welding speeds ($R_p < 10^{-3/2}$), and also for very fast travel speeds ($R_p > 1$). Between these limit cases, a more complicated function approximates the dependence [22], so a relation of the type [4] is always available. The significance of this relation is that [4b] can give r_∞ , and that value substituted into [1] and [3] to give the needed auxiliary power $P_a = P_{tot} - P_d$, given by:

$$\frac{P_a}{P_d} = \frac{6\kappa_d t_d}{d_d^2}\left(\frac{2r_\infty}{d_d}\right)\frac{T_m}{T_{\sup}}\left(\frac{k}{k_d}\right) - 1 \qquad [5a]$$

which can be rewritten for clarity in terms of the dimensionless quantities

$\varepsilon = \dfrac{d_d k_d T_{\sup}}{2pkT_m}$ and $\delta = \dfrac{4\kappa_d t_d}{d_d^2}$, taking the form

$$\frac{P_a}{P_d} = \frac{3\delta}{2\varepsilon}\,\frac{r_\infty}{p} - 1 \qquad [5b]$$

In [5b], the ratio $\dfrac{r_\infty}{p}$ is supplied by [4b,c] while ε and δ are independent parameters with known values when the droplets and penetration are set.

The wire feed V_w is also determined by these parameters, of course:

$$V_w = \frac{2}{3}\left(\frac{d_d}{d_w}\right)^2 \frac{d_d}{t_d} \qquad [6]$$

in terms of the droplet parameters and the wire diameter d_w .

Now Eqs.[2] [5] and [6] give the operating conditions needed to produce the desired penetration using the specified droplet stream. Eqs.[2,5,6] conserve mass and energy globally, but they do not include any dynamics or heat transfer rate at the droplet/workpiece interface, so they should be considered necessary conditions for the micro-GMAW bead deposition to succeed, but cannot be regarded as sufficient conditions to guarantee that the combination will work.

These relations require some discussion. By replacing [2] with its dimensionless counterpart:

$$R_p = V_o\ p\ /\ 2\ \kappa = (1 - f_{ol})\, d_d\ p\ /\ 2 t_d\ \kappa \qquad [2b]$$

we now have a completely dimensionless formulation with δ , ε and R_p being the independent variables, and the values of $\dfrac{r_\infty}{p}$ and $\dfrac{P_a}{P_d}$ being determined from them by [4c] and [5b]. The parameter δ is the ratio of heat conduction penetration distance between droplet arrivals to the droplet size, so $\delta > 1$ assures that there is time enough to conduct the heat out of the droplet before the next droplet arrives. The value ε is the ratio of (power required to maintain a steady pool size equal to the penetration)/ (power deposited, from the droplet superheat). Finally, R_p discriminates between fast, slow and intermediate welding speeds, and fixes the power requirement through [4b,c].

To construct the example in Fig. 4.1, given the values in the caption and definition [2b], we have δ = 5.73 and ε = 1.18 with R_p = 0.11076. This R_p value is in the intermediate range in [4c],

so the value of F(R_p) is calculated to be $\frac{r_\infty}{p}$ = 1.068. Thus, [5b] gives $\frac{P_a}{P_d}$ = 6.79, or P_a = 31.2 W. This case is illustrated in the figure.

From [5b], it is clear that the auxiliary power required can be reduced if we use smaller values for δ or larger values for ε. In the Fig. 4.1 example, δ = 5.73 is a conservative value, so decreasing t_d to 0.0035 sec (290 Hz) would reduce that to δ =1, which should still be safe for heat conduction because of the internal motions of the droplet. Changing t_d would also change travel speed in [2], .so that V_o =6.43 cm/sec (152 ipm) and consequently the Rykalin number is R_p = 0.633, in the region where [4c] must be used to evaluate $\frac{r_\infty}{p}$ = 1.607. Then we determine $\frac{P_a}{P_d}$ = -0.5105, the negative value indicating that this δ, t_d choice will in fact produce greater penetration than specified, because the droplets carry more heat than needed.

The relations [2b],[4b,c],[5b] implicitly define welding parameters for which auxiliary power is zero. To identify these conditions systematically, we note that [5b] would require

$$\frac{r_\infty}{p} = \frac{2\varepsilon}{3\delta} > 1$$

so that [4c] gives a map of the possible dimensionless parameters which will have Pa=0, see Fig. 4.3. Knowing this relationship, one readily computes the dimensioned parameters needed to make such a weld

Some Considerations of Interface Conduction:

a. MicroGMAW with a solid workpiece. Suppose a droplet sticks to a cold workpiece (sheet of thickness h) in the form of a hemisphere of diameter d . If its initial temperature was T_2 and the workpiece was at T_o, calculate first the temperature T_1 which droplet and a plug of the workpiece , of volume V_w, will reach if conduction makes them isothermal while leaving the remainder of the workpiece at the initial temperature T_o. Result:

   Let $C_d = \rho_d C_{pd} V_d$ and C_w = corresponding term for the workpiece volume V_w. Then, in terms of these known quantitites:

   $$T_1 - T_0 = (T_2 - T_0)/(1 + C_d / C_w)$$

   When the heated volume V_w of the workpiece is in the shape of a truncated cone of diameter d1 on the workpiece topside, and diameter d2 on the workpiece bottom, the ratio C_d / C_w becomes

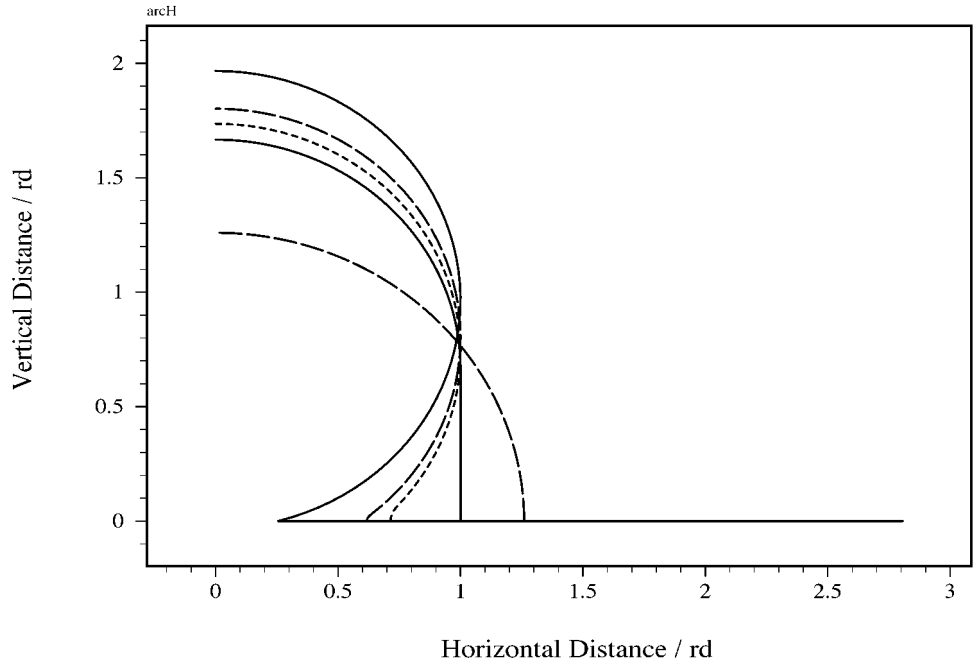

Fig. 4.2. Droplet Envelope Shapes during Collision. Collsion starts from a spherical droplet, and conserving volume between a tangent hyperboloid and the sphere. First phase ends when hyperboloid becomes straight line (4^{th} curve from top) after 1/3 radius of penetration. The second phase evolves from this cylinder+ hemisphere shape into a hemispherical button of 1.26 times the initial radius (lowest dashed curve).

One could go along with this deposition, so long as travel speed keeps the heated workpiece volumes from overlapping. Then Vo period > r1 is required….

b. LENS on a molten workpiece: When the droplet is absorbed into an already molten pool, its heat is added to the heat already there, and fluid motion aids in distributing this heat over the pool volume. The net effect can be imagined as an increase in the pool volume and the volume of heated workpiece, and therefore an increase of travel speed for the pool of about dl/period where period is droplet repeat time and dl is dvol/area with area being the transverse area of pool plus HAZ (roughly).

Droplet Collison Kinematics

Consider the collision of a droplet impinging along the normal to a solid plane surface. The geometry of morphing from a flying spherical droplet into an attached hemispherical button requires considerable internal flow in the droplet. Just how much deformation must occur can be assessed by asking "How different is the envelope of the sphere and the intermediate shapes, if the contact angle is 90 degrees, and the total volume is the same for each shape?" When the transition from the plane to the sphere is a hyperboloid of revolution, tangent to the sphere, for the penetration of radius/3, this hyperboloid has become a cylinder. So there are three key shapes here: the original sphere just at contact, the cylinder+hemisphere (both of the original radius r_d), and finally the hemisphere (of $r_d \sqrt[3]{2}$). As Fig. 4.2 shows, these are not huge

adjustments of the surface tension membrane, and do not have to impose huge flows on the contents. In fact, the hyperboloids indicate that the surface tension will strongly aid the initial flow, which moves fluid radially outward, because they have a small radius of curvature which sustains a large pressure drop between ambient and the droplet interior.

These shapes are not pictures of the actual collision, however. No flow computation was done for them, only the volume-conserving geometry. The fluid motions required to change one shape to the next would violate Newton's laws, and the fluid would still be in motion as it reached the 'final' shape. Surface tension would have to confine it after this time, and viscosity would have to damp out these residual motions. Thus, there can only be a narrow range of approach speeds which allow even an approximate match with these shapes.

To get an idea of how large this speed could possibly be, we can say that the surface tension must contain the liquid after the collision. Further, the acceleration required to do this can be estimated (judging from the basketball bounces visible in the VHS) by assuming the drop wants to come off the surface with the approach velocity reversed (that is, viscous damping is neglected on the first oscillation). That means average acceleration of $V_o/(r_d/V_o)$ for a drop of radius r_d approaching at V_o. If the surface tension force $2\ \pi\ r_d \sqrt[3]{2}\ \sigma$, where σ = surface tension, is to provide this acceleration, then

$$V_o \leq 2.18 \sqrt{\sigma / \rho r_d} \qquad [1]$$

If we forget the 2.18 factor, 33 cm/sec is a working upper bound. This gives an idea of what timescales r/V_o are relevant, namely, 3 msec, and accelerations are then around 11 X Earth's g. This is not excruciating.

If the collision decelerates at 11 g, and winds up with a liquid drop of radius $r_d\ \sqrt[3]{2} \sim 1.26\ r_d$, we can also consider the heat conduction during each phase of the collision. Start with the Philips case, high conductivity in the droplet, much less in the workpiece. Then the droplet has time to keep more or less isothermal as the workpiece heats. For steel, with k ~ 0.3 W/cm-K and diffusivity κ_w = 0.06 cm^2/sec, the heating penetrates about $\sqrt{4\kappa_w \Delta t}$ = 0.26 mm, a depth comparable to the droplet size, during the collision time, 3 msec. Because of this speedy heatup in the immediate vicinity of the drop, we lose the one-dimensional estimate of the interface temperature (temperature rise in proportion to (κ_d / κ_w) X $(T_d(0) - T_w(0))$ where $T_d(0)$ is initial droplet temperature and $T_w(0)$ initial workpiece T), but it still serves as an upper bound on interface temperature.

The implication is that a droplet superheated above the melt point of the workpiece can be expected to bring some small volume to melt, during the collision process itself. If the superheat is great enough, the melted volume of workpiece can approach that of the droplet. All this matches the Philips specimen, in that the backside HAZ (discolored region) seems to stay quite close to the droplet size.

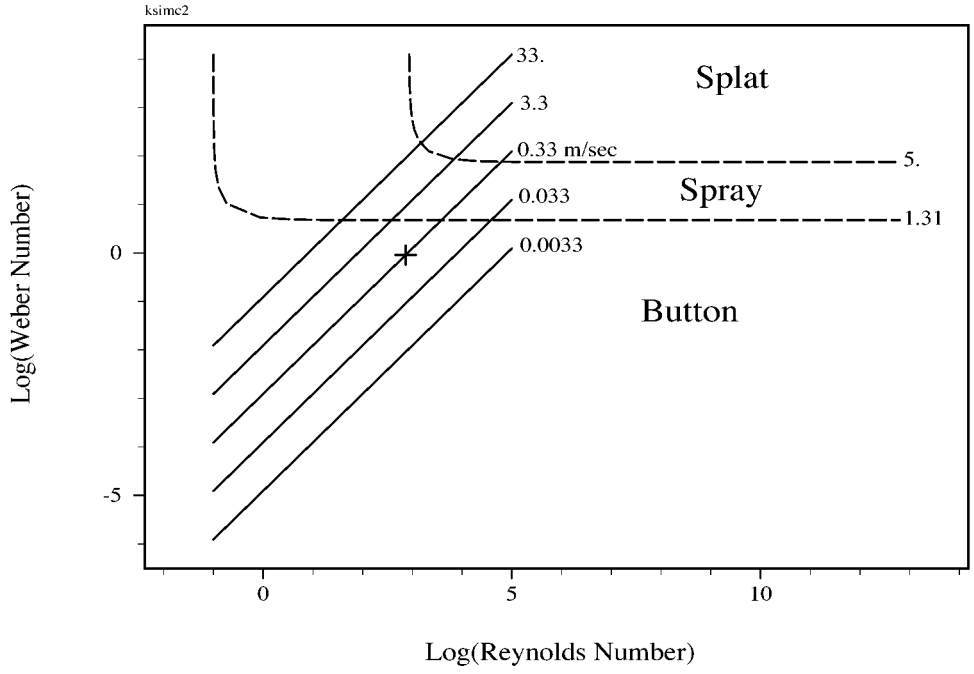

Fig. 4.3. Log-Log plot of Weber number We vs Reynolds number R_e for droplets with given values of the dimensionless parameter $P = V_o\ \mu / \sigma$ (parallel lines of slope 1). The parallel lines are made up of points with different droplet sizes d_d, but with the same (scaled) collision velocity V_o. The dashed curves represent equal final deformation contours, with values of ξ_m =1.31 and ξ_m =5. Plot symbol + denotes 1.25 mm dia droplet on Philips sample.

Droplet Collison Dynamics

There is a literature assessing the dynamics of the droplet as it collides with a substrate. Sirignano [24] gave a recent review of simulations; along another parallel branch, Trapaga and Szekely [25] considered isothermal droplets, using both computational fluid dynamic (CFD) simulation and calibrating experiments. This work can be summarized by noting that the key forces at work on the fluid in the droplet are inertial, viscous and surface tension forces. Thus, the dimensionless numbers which capture the intertial/viscous (Reynolds number $R_e = V_o\ d_d\ / \nu$) and inertial/surface tension (Weber number, $We = V_o^{\,2}\ d_d\ \rho / \sigma$) force ratios can be used to identify the type of collision to be expected. Using a geometrically crude approximation, Madejski [26] obtained a closed form expression for the overall diameter of the splat, which he called $\xi_m = d_s / d_d$. Contours of this parameter for ξ_m =2 and ξ_m =5 are shown in Fig. 4.3 The first of these, ξ_m =2, is near to the Philips case, which has ξ_m =1.26, and represents an upper bound on collision speeds which will allow a droplet to form the hemispherical final shape, as opposed to a "splat" condition in which the deformation spreads the droplet thinly over several diameters. Since inertia forces are relatively stronger in Fig. 4.3 to the right and upward, it is the conditions to the lower left for which the hemispherical shape is feasible.

For the Philips case [19], with V_o =33 cm/sec, Cu at the melting point of carbon steel (1675 K) will have viscosity 4.5e-3 Pa-sec and surface tension 1.2 N/m. Thus $P = V_o\ \mu / \sigma$ = 1.24e-3 defines a line in Fig 4.3 along which lie the three droplet sizes appear as points. One such point has R_e = $V_o\ d_d\ / \nu$ = 730 or so for droplet diameter of 1.25 mm. The corresponding $We = P\ R_e$ = 0.91 indicates that surface tension is the same scale as inertial force for this droplet. The much larger than unity value of the Reynolds number indicates that viscosity is too weak to damp the fluid flow during the collision, so a movie of the collision would no doubt show several oscillations of the droplet before viscosity and solidification ended the motions in the final button. The largest Philips droplets, with about 2mm dia, lie at (R_e , We) = (1200,1.45) and can be described in the same qualitative terms; i.e., these are in the same dynamic regime ('Button') as the smallest droplets of the Philips sample.

A final dynamics issue is the sensitivity of the interfacial conditions (between droplet and deposition surface) to the chemistry. Surface tension in metals is extremely sensitive to trace amounts of surfactant, and many metal oxides are surfactants. Similarly, the contact angle of the droplet surface tension membrane with the surface depends on chemistry, so the basic dynamics outlined above can be expected to change dramatically when trace amounts of surfactant are present at the interface. The same will be seen to be true of the heat transfer across the interface—surface chemistry can alter the interface resistance to heat flow between drop and substrate. Thus, investigation of chemical conditions is necessary to characterize these collision processes.

Solidifying Droplet Collison Dynamics

When the liquid of the droplet freezes during the collision process, the dynamics can be affected. Madejski [26] investigated this aspect of the problem analytically, and Trapaga et al. [27] treated it in their numerical solutions. Its appearance in the problem introduces the Prandtl number $P_r = \nu / \kappa$ to characterize the viscous diffusion /thermal diffusivity ratio (P_r = 0.04 for Cu) However, Madejski found it more convenient to define a specialized 'solidification parameter' k by:

$$k = \frac{3}{2} U \frac{\rho_s}{\rho} \sqrt{\frac{1}{2 \,\mathrm{Pr}\,\mathrm{Re}}}$$

where U = (local solid layer thickness / $\sqrt{\kappa_s t}$ is a constant in Madejski's treatment (See Hill [28]), and subscript 's' denotes solid. Superheat does not appear here because he sought to keep Tsup = 0 in his experiments, which covered parameter ranges:

1.1e4 < Re < 1.5e5

25 < We < 7.3 e 3

70 < Pr Re < 1.3 e 3

$0.035 < k < 0.16$.

For the Philips sample at zero superheat, k = 0.09, and PrRe = 28. Thus, our case differs from the literature in being below the values of all the dimensionless numbers except the freeze parameter, and that matches only when superheat is ignored. All these differences move the relative sizes of the forces toward the conditions favoring droplet sticking and taking on a hemispherical shape rather than spreading out into a "splat". Trapaga et al. [27] and Hofmeister et al. [29] have done considerable simulation with thermal data from experiments to calibrate the effects of solidification. Results are all in regions of interest to spray technologies, that is, the regime mapped by Madejski, and tend to elaborate his conclusions without fundamentally altering them.

To summarize, our interest is in the lower left of Fig.4.3, while the literature has treated the upper right, where the droplet spread is approximated by:

$$\xi_m = 1.5344\ k^{-0.395}$$

Perhaps there is a literature in the solder technology area which examines We = o(1) and Re < 10, but we have not yet identified it. SNL resources in elaboration on Fig. 4.1 may include the Surface Evolver code, as well as the experimental facilities in the Weld Lab.

Appendix:

Software. The Madejski results in Fig.4.3 are generated with a FORTRAN program 'WeRe.f', and plotted with 'XPLOT' from the file automatically generated. WeRe is interactive, and calls for the inputs noted below: viscosity, surface tension, density, temperature to characterize the droplet alloy. It then calculates and reports (in 'fort.66' output file) the derived values, and writes the plot files for XPLOT. The names of the plot files and their content can be seen in the file 'xbd' which is written to direct the plot.

Sample 'fort.66' Output File:

```
For     1.25000E-03 dia droplets with properties:
    viscosity=    4.50000E-03 Pa-sec.
    surface tension=    1.20000 N/m.
    density=    8000.00 kg/m**3.
    at temperature    1700.00 K,
    colliding with speed   0.330000 m/sec,
    dimensionless numbers are:
    Reynolds number=    733.333 and Weber number=   0.907500.
  KSIM modified input to rksi1=    1.30721
 ksim,r1,w1,boyR=    1.30721   -1.00000   0.677862    4.09255
 r2,w2,vert,horiz,Remax= -0.999833    4.09255   10.00000    13.8000    12.8000
 ksim,r1,w1,boyR=    5.00000    2.93453    1.87506    4.09255
 r2,w2,vert,horiz,Remax=    2.93717    4.09255   10.00000    13.8000    12.8000
```

Appendix 1. Relation [4c] can be written as

$$\log\left(r_\infty / p\right) = \frac{2}{25}\left(\log R_p + 3/2\right)^2 + \frac{4}{125}\left(\log R_p + 3/2\right)^3$$

that is, a polynomial fit to the log-log plot of F(R_p) with the Rykalin number as independent variable. Fortunately, this is simple enough to be solved in general for R_p in terms of r_∞ / p, as follows:

Let $x = 27 \log\left(r_\infty / p\right) - 1$; then for the range of R_p covered by the fit in [4c], x is in $-1 < x < 26$, and the solution takes one of two forms: .

$$\log R_p = \frac{5}{6}\left\{ \left[x + \sqrt{x^2 - 1}\right]^{1/3} + \left[x - \sqrt{x^2 - 1}\right]^{1/3} \right\} - \frac{4}{3} \quad \text{for } x > 1;$$

or

$$\log R_p = 2 \cos\left(\frac{1}{3}\cos^{-1} x\right) \quad \text{for } x < 1 .$$

Summary

The hoped for advantages of laser assist for gas metal arc welding were not obtained with the small diameter wire employed in this study. The physical constraints to consistent detachment with small droplets were not overcome with the many experimental approaches investigated. Encouraging results were obtained with servo dip transfer but the process is complex and the advantages were not significant enough to warrant continued development. The use of high arc power to detach the small diameter wire reliably was demonstrated in this study but the negative effect of high power on workpiece heating was considered to be an impractical result, and no significant investigation with that approach was attempted either.

Without achieving successful micro wire welding, the advantages of laser assist could not be investigated and the project was discontinued. These results do not apply to gas metal arc welding at high arc power with laser assist, since the advantage of a supplementary focused heat source is more pronounced at high arc powers, and may yet prove beneficial in high volume manufacturing.

References

1. Duley, W. W. *Laser Welding* (John Wiley & Sons, New York, 1999).
2. Dupont, J. N. & Marder, A. R. Thermal Efficiency of Arc Welding Processes. *Welding Journal* **74**, 406s-416s (1995).
3. Fuerschbach, P. W. & Hinkley, D. A. Pulsed Nd:YAG Laser Welding of Heart Pacemaker Batteries with Reduced Heat Input. *Welding Journal* **76**, 103s-109s (1997).
4. Lancaster, J. F. *Metallurgy of Welding* (George Allen and Unwin, London, 1980).

5. Abe, N., Kunugita, Y., Hayashi, M. & Yoshiaki, Y. Dynamic Observation of High Speed Laser-Arc Combination Welding of Thick Plates. *JWRI* **26** (1997).
6. Wendelstorf, J., Decker, I. & Wohlfahrt, H. Laser Enhanced Gas Tungsten Arc Welding. *Welding in the World* **34**, 395-396 (1994).
7. Beyer, E. et al. in *ICALEO* 183-192 (1994).
8. Fuerschbach, P. W. in *ICALEO 99* (LIA, San Diego, CA, 1999).
9. O'Brien, R. L. (ed.) *Welding Processes,Welding Handbook, Vol 2* (AWS, Miami, FL, 1991).
10. Mesyats, G. A. *Ectons* (Nauka, Ekaterinburg, Russia, 1993).
11. Shmelev, D. L. & Litvinov, E. A. in *IEEE 18th Symp. On Discharges and Elec. Insulation in Vac.* P73 (Eindhoven, 1998).
12. Watkins, A. D. & Smartt, H. B. in *Recent Trends in Welding Science and Technology* (ed. S.A. David and J.M. Vitek, e.) p. 19 (ASM International, Materials Park, OH, 1990).
13. Kim, Y. S. & Eagar, T. W. in *Recent Trends in Welding Science and Technology* (ed. S.A. David and J.M. Vitek, e.) p. 13 (ASM International, Materials Park, OH, 1990).
14. Suslov, A. V., Dreizin, E. L. & Trunov, M. A. Formation of monodisperse refractory metal particles by impulse discharge. *Powder Technology* **74**, 23-30 (1993).
15. Naidenov, A. M. Mechanical Control of the Transfer of Electrode Metal. *Avt. Svarka*, 31-33 (1969).
16. Voropai, N. M., Savelev, O. N. & Semergeeev, S. S. Electromanetic Mechanisms for the Pulsed Feed of Welding Wire. *Avt. Svarka*, 46-49 (1980).
17. Tarasov, N. M. Droplets of electrode metal broken away by brief gas jets. *Avt. Svarka* **39**, 10-13 (1986).
18. Jones, L. A., Eagar, T. W. & Lang, J. H. in *International Conference on Trends in Welding Research* 1009-1013 (ASM, Gatlinberg, Tn, 1992).
19. Buelens, J. J. C. (Science and Technology of Welding and Joining, vol.2, no.6. 1997. pp.239-243. 9 fig., 4 ref., 1997).
20. Brooks, J. A. et al. (Sandia National Laboratory, 2001).
21. Christensen, N., Davies, V. L. & Gjermundsen, K. Distribution of Temperatures in Arc Welding. *British Welding Journal* **12**, 54-75 (1965).
22. Fuerschbach, P. W. in *4th Intl. Conf. on Trends in Welding Research* (ASM Intl., Gatlinburg, Tenn., 1995).
23. Bertram, L. A. (Sandia National Laboratories, 1996).
24. Sirignano, W. A. *Fluid Dynamics and Transport of Droplets and Sprays* (Cambridge University Press, New York, 1999).
25. Trapaga, G. & Szekely, J. Mathematical Modeling of the Isothermal Impingement of Liquid Droplets in Spraying Processes. *Metall. Trans. 22B*, 901 (1991).
26. Madejski, J. Solidification of Droplets on a Cold Surface. *Int. J. Heat Mass Transf.* **19**, 1009 (1976).
27. Trapaga, G., Mathhys, E. F., Valencia, J. J. & Szekely, J. Fluid Flow, Heat Transfer, and Solidification of Molten Metal Droplets Impinging on Substrates: Comparison of Numerical and Experimental Results. *Metall. Trans.* **23B**, 701 (1992).
28. Hill, J. M. *One-Dimensional Stefan Problems: An Introduction* (Longman Scientific & Technical/Wiley & Sons, New York, 1987).

29. Hofmeister, W., Bayuzick, R. J., Trapaga, G., Matson, D. M. & Flemings, M. C. in *Solidification 1998* (ed. Marsh, S., Dantzig, J., Tivedi, A., Hofmeister, W., Chu, Lavernia and Chun) p.375 (TMMMS, Warrendale, PA., 1998).